Available online at www.sciencedirect.com

ScienceDirect

www.elsevier.com/locate/jes

JES JOURNAL OF ENVIRONMENTAL SCIENCES

www.jesc.ac.cn

One-pot synthesis of Fe/Cu-SSZ-13 catalyst and its highly efficient performance for the selective catalytic reduction of nitrogen oxide with ammonia

Jie Wan[1], *Jiawei Chen*[2], *Ru Zhao*[2], *Renxian Zhou*[2,*]

[1] *Energy Research Institute, Nanjing Institute of Technology, Nanjing 211167, China*
[2] *Institute of Catalysis, Zhejiang University, Hangzhou 310028, China*

ARTICLE INFO

Article history:
Received 8 June 2020
Revised 5 August 2020
Accepted 5 August 2020
Available online 14 August 2020

Keywords:
NH_3-SCR
Fe/Cu-SSZ-13
One-pot synthesis
Active species

ABSTRACT

Series of Fe/Cu-SSZ-13 catalysts with different Fe loading content were synthesized by simple one-pot strategy. The obtained catalysts were subjected to selective catalytic reduction (SCR) of NO_x with NH_3 and were characterized by various techniques. The results show that $Fe_{0.63}/Cu_{1.50}$-SSZ-13 catalyst with proper Fe content exhibits excellent catalytic activity with widest operation temperature window from 160 to 580°C, excellent hydrothermal stability as well as good resistance to sulfur poisoning when compared with Cu-SSZ-13, signifying its great potential for practical applications. Further characterizations reveal that the synthesized Fe/Cu-SSZ-13 catalysts present typical chabazite (CHA) structure with good crystallinity, while isolated Cu^{2+} and monomeric Fe^{3+} are revealed as the predominant copper and iron species. At low temperatures, isolated Cu^{2+} species act as primary active sites for SCR reaction, while monomeric Fe^{3+} species provide sufficient active sites for sustain the SCR activity at high temperature. Moreover, Fe over doping would lead to the damage of zeolite structure, destruction of isolated Cu^{2+} site, as well as the formation of highly oxidizing Fe_2O_3, thus causing deterioration of catalytic performances.

Introduction

Nitrogen oxides (NO_x), as one of the major toxic pollutants exhausted from diesel engine vehicles and fossil-fuel power plants, have long been considered leading cause for photochemical smog, ozone depletion and acid rain (Busca et al., 1998; König et al., 2001). Among all the denitrification ($deNO_x$ or NO_x elimination) techniques, selective catalytic reduction of NO_x using ammonia as reductant (NH_3-SCR) has been recognized as the most efficient way for NO_x elimination of diesel engine emissions especially under lean condition (García-Cortés et al., 2001; Epling et al., 2004; Si et al., 2010). The first-generation NH_3-SCR catalysts V_2O_5-WO_3/TiO_2 have been successfully commercialized and widely employed in denitrification systems since 1970. However, it still faces serious challenges such as narrow operation temperature windows, poor thermal stability, low resistance to sulfur as well as toxicity of V^{5+} species (Li et al., 2011; Zhang et al., 2019). As the emission regulations become more and more stringent, demand for developing new SCR catalysts remains urgent and have drawn much effort both in academia and industry.

Zeolite supported copper catalysts, such as Cu-beta, Cu-ZSM-5 and Cu-SAPO-34 have been extensively studied for NH_3-SCR reaction over the past few years (Qi et al., 2008; Wang et al., 2012; Liu et al., 2016). Among many zeolites investigated, Cu-exchanged SSZ-13 zeolite with chabazite (CHA) structure has been currently state-of-the-art cata-

* Corresponding author.
E-mail: zhourenxian@zju.edu.cn (R. Zhou).

https://doi.org/10.1016/j.jes.2020.08.003
1001-0742/

lyst that attracted lots of attention recently. Several studies have confirmed that Cu-SSZ-13 exhibited outstanding activity for NH_3-SCR, superior N_2 selectivity and good hydrothermal stability compared to Cu-beta and Cu-ZSM-5 (Gao et al., 2017; Chen et al., 2018). It also shows good resistance to unburnt hydrocarbons, which benefits its practical operation for the diesel engine vehicle. On the other hand, SCR activity over high temperature range is also extremely desirable for NO_x elimination as the engine exhaust can be quite heated-up during acceleration (Gao et al., 2015a). While Cu/SSZ-13 catalysts give unsatisfactory SCR selectivity above 300°C, Fe/zeolites presents clear advantages for high-temperature SCR performances. For example, Gao et al. (2015b), Shishkin et al. (2014) and Wen et al. (2015) all reported that Fe-SSZ-13 showed better activity and N_2/N_2O selectivity during SCR test above 350°C. Thus, from the purpose of making complementary advantages of both Cu and Fe zeolites, a combined hetero-bimetallic Cu/Fe-SSZ-13 system might provide optimized NH_3-SCR performance at expanded temperature range. The correlations between active metal species and catalytic performance need further exploration as well.

Moreover, the preparation of mono/bi-metallic SSZ-13 catalysts have long been complicated. Conventional synthesis of SSZ-13 zeolite reported by Zones and Vannordstrand (1988) involves usage of expensive organic compound (N,N,N-trimethyl-1-adamantammonium hydroxide, TMAdaOH) as template. The as-synthesized SSZ-13 zeolites require post ion exchange procedures to obtain Cu-SSZ-13. Ren et al. (2011) proposed simple one-pot synthesis of Cu-SSZ-13 by employing Cu^{2+}coordinated with copper-amine complex. Subsequently, further improvement for the one-pot synthesis of Cu-SSZ-13 catalyst have been conducted. As for the bimetallic FeCu-SSZ-13 catalysts, the preparation process includes synthesis of Na-form Cu-SSZ-13, transformation of Na-form Cu-SSZ-13 into H-form Cu-SSZ-13, ion exchange of Fe^{3+} into H-form Cu-SSZ-13 (Zhang et al., 2015; Wang et al., 2019), and such multiple complex ion-exchange processes remains big challenges and are unfavorable for future industrial application. Therefore, it is also urgent desired to develop low-cost, controllable, and reproducible one-pot strategy for Fe/Cu-SSZ-13 synthesis.

In the present study, Fe/Cu-SSZ-13 catalysts with different Fe loading content were synthesized by simple one-pot strategy. The obtained catalysts were evaluated for NH_3-SCR catalytic performances and characterized by various techniques. The scope of this paper is to (i) to report a more effective one-pot synthesis strategy for preparing bimetallic Fe/Cu-SSZ-13; (ii) to obtain Fe/Cu-SSZ-13 catalysts with satisfactory activity and stability for NH_3-SCR reaction by regulating active components; and (iii) so as to acquire new insights regarding the structure-activity relationship of Fe/Cu-SSZ-13 catalysts for NH_3-SCR reaction.

1. Materials and methods

1.1. *Catalysts preparation*

Fe/Cu-SSZ-13 catalysts with different Fe content were prepared by one-pot procedures as follows: (I) quantitative amount of $CuSO_4 \cdot 5H_2O$ was first dissolved and stirred in deionized water for 30 min; (II) 1.2 g tetraethylenepentamine (TEPA) was then added and stirred for 60 min; (III) certain amount of NaOH, $NaAlO_2$ and $K_4Fe(CN)_6 \cdot 3H_2O$ was added sequentially and stirred for another 60 min; (IV) 3.6 mL silica sol was added drop by drop to the above solution under vigorous stirring for 3 hr; (V) the mixture was then transferred a Teflon-lined autoclave and underwent hydrothermal treatment at 140°C for 96 hr; (VI) the obtained product was filtered, washed, dried at 100°C for 12 hr and then further acid-leached in the HNO_3 solution at 80°C for 12 hr; (VII) the dried solid was calcined in a muffle furnace at 550°C for 4 hr to obtain the desired catalysts.

The molar ratio of each component in the synthesis system was 5 Na_2O: Al_2O_3: 300 H_2O: 10 SiO_2: 2.5 Cu-TEPA: x $K_4Fe(CN)_6 \cdot 3H_2O$ (x = 0, 0.06, 0.1, 0.13, 0.16). The mole ratio of Cu-TPEA/Al_2O_3 was 2.5, while the different introducing amount of Fe was controlled by changing the quantity of $K_4Fe(CN)_6 \cdot 3H_2O$. The Fe/Cu content in the obtained Fe/Cu-SSZ-13 catalysts were determined by inductively coupled plasma-atomic emission spectrometry (ICP-AES) tests using IRIS Intrepid IIXSP spectrometer (IRIS Intrepid IIXSP, Thermo Scientific, USA) and the synthesized catalysts were designated based on the ICP-quantitative results as $Cu_{3.25}$-SSZ-13, $Fe_{0.40}/Cu_{1.65}$-SSZ-13, $Fe_{0.53}/Cu_{1.55}$-SSZ-13, $Fe_{0.63}/Cu_{1.50}$-SSZ-13 and $Fe_{0.79}/Cu_{0.56}$-SSZ-13 respectively (the number is subscript stands for weight percentage).

To further evaluating the hydrothermal stability of the obtained Fe/Cu-SSZ-13 catalysts, certain selected samples were treated in air-steam flow with 10 vol.% H_2O of 25.0 mL/min at 750°C for 24 hr to obtain the hydrothermal aged catalysts (designated as -aged). Similarly, certain selected samples were treated in 100 ppmV SO_2/Ar gas flow at 350°C for 16 hr to obtain the sulfur-poisoned catalysts (designated as -SO_2), in order to further evaluate the sulfur-resistance of the obtained catalysts.

1.2. *Catalysts characterizations*

X-ray diffraction analyses (XRD) were conducted on X-ray diffractometer using Cu $K\alpha$ radiation (XRD-7000, Shimadzu, Japan). The tube voltage sets at 40 kV and tube current sets at 30 mA. The diffractograms were records in with 0.02° step size the range from 10° to 140° (2θ).

H_2 temperature-programmed reductions (H_2-TPR) were conducted in the fixed-bed reactor using thermal conductivity detector (Chembet 3000, Quantachrome, USA). First, 100 mg catalyst was purged in N_2 flow (30 mL/min) at 400°C for 0.5 hr. After cooling to room temperature, 40 mL/min 5 vol.% H_2/Ar flow was introduced till the baseline was stable. Then, the H_2-TPR profile was recorded while the reactor temperature was simultaneously raised to 1000°C (heating rate 10°C/min).

X-ray photoelectron spectroscopies (XPS) were conducted on a Thermo ESCALAB 250 apparatus using mono-chromated Al $K\alpha$ radiation (ESCALAB 250, Thermo Scientific, USA). The binding energies were calibrated according to the C 1 s peak (284.8 eV) as internal labeling.

Ultraviolet visible spectra (UV–Vis) were collected on an UV-2450 spectrometer (UV-2450, Shimadzu, Japan). The wave-

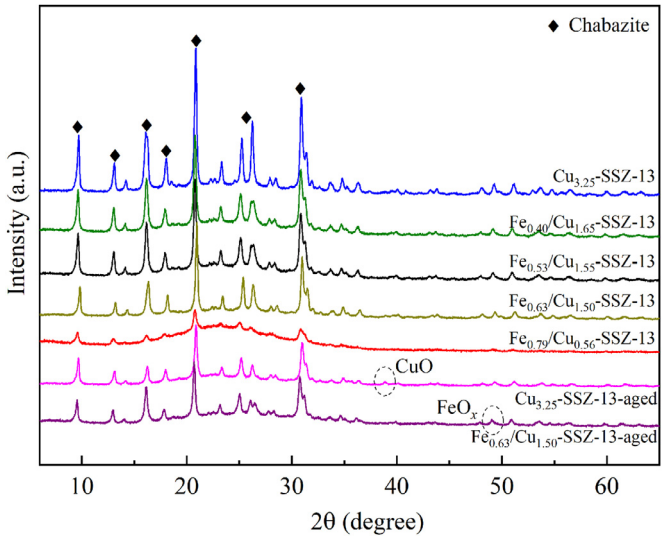

Fig. 1 – X-ray diffraction (XRD) patterns of the obtained and hydrothermal aged Fe/Cu-SSZ-13 catalysts.

length range was from 200 to 800 nm at room temperature using $BaSO_4$ as reference.

1.3. *Catalytic activity tests*

NH_3-SCR activity tests were evaluated in a fixed-bed quartz reactor. The reaction mixture consists 500 ppmV NO_x (490 ppmV NO mixed with 10 ppmV NO_2), 500 ppmV NH_3, 5 vol.% O_2 and Ar as balancing gas (total gas hourly space velocity (GHSV) 50,000 hr^{-1}). Concentrations of both inlet an exhaust gas (NO, NO_2, N_2O, NH_3) were quantitatively monitored by a Bruker EQUINOX 55-FTIR spectrometer (EQUINOX 55, Bruker, Germany). NO_x and NH_3 conversions were determined according to the following Eqs. (1) and (2):

$$C_{NO_x} = \frac{NO_{x-inlet} - NO_{x-outlet}}{NO_{x-inlet}} \times 100\% \quad (1)$$

$$C_{NH_3} = \frac{NH_{3-inlet} - NH_{3-outlet}}{NH_{3-inlet}} \times 100\% \quad (2)$$

where, C_{NOx} (%) and C_{NH3} (%) are the conversion of NO_x and NH_3, respectively; $NO_{x\text{-inlet}}$ (ppmV) and $NO_{x\text{-outlet}}$ (ppmV) are the NO_x concentration before and after the SCR reaction test, respectively; $NH_{3\text{-inlet}}$ (ppmV) and $NH_{3\text{-outlet}}$ (ppmV) are the NH_3 concentration before and after the SCR reaction test, respectively.

2. Results and discussion

2.1. *Crystalline structures by XRD analyses*

XRD analyses were conducted to validate the crystalline structures of the synthesized Fe/Cu-SSZ-13 catalysts. Fig. 1 shows the obtained XRD patterns. All the catalysts presented characteristic peaks (2θ) at 9.5°, 14.0°, 16.1°, 17.8°, 20.7°, 25.0° and 30.7°, which are feature diffraction peaks of typical chabazite (CHA) structure of SSZ-13 zeolites (Wang et al., 2015; Zhang et al., 2015). Sharp peak with relatively high intensity can be observed in all the catalysts except $Fe_{0.79}/Cu_{0.56}$-SSZ-13 catalysts, representing good crystallinity formed in Fe/Cu-SSZ-13 with proper Fe content. It can be clearly demonstrated that the one-pot method applied was quite successful in synthesis of Fe/Cu-SSZ-13 with CHA structure. With increasing Fe content, the main peak (211) (around 20.73°) decreased gradually, indicating that Fe content can affect the relative crystallinity of the Fe/Cu-SSZ-13 molecular sieve. Such decrease in crystallinity demonstrated that some of the Fe species has been introduced into the molecular sieve framework. For $Fe_{0.79}/Cu_{0.56}$-SSZ-13, the weakened and broaden CHA diffraction peaks indicate its zeolite structure could be severe damaged due to Fe over-doping. No diffraction peaks related to CuO (at $2\theta = 35.6°$ and 38.8°) or FeO_x (at $2\theta = 35.6°$, 49.5°, 54.1° and 62.5°) were observed, which can be either related to the low content beyond detection limit or the well distribution of copper/iron species into the zeolite matrix (Nares et al., 2002; Deka et al., 2012). XRD profiles of hydrothermal aged $Cu_{3.25}$-SSZ-13 and $Fe_{0.63}/Cu_{1.50}$-SSZ-13 catalysts were also presented in Fig. 1. As can been seen, typical diffraction peaks of CHA structure can be maintained fundamentally after hydrothermal aging, indicating the zeolite structure was not severely destroyed. However small CuO and FeO_x can be observed after hydrothermal aging, indicating the migration/agglomeration of both copper and iron species occur during the hydrothermal aging.

2.2. *Redox properties by H_2-TPR analyses*

H_2-TPR is commonly used to characterize the redox properties of the catalysts. The obtained H_2-TPR profiles are shown in Fig. 2. For $Cu_{3.25}$-SSZ-13 catalyst, multiple reduction peaks can be observed below 500°C and around 700°C. Three reduction peaks (α, β, and γ) below 500°C represent the reduction of isolated Cu^{2+} species in the SSZ-13, as these Cu^{2+} species are coordinated in various sites of the CHA structure and presented correspondingly different reduction abilities (Appendix A **Fig. S1**). Peak α (181°C) can be assigned to the reduction of isolated

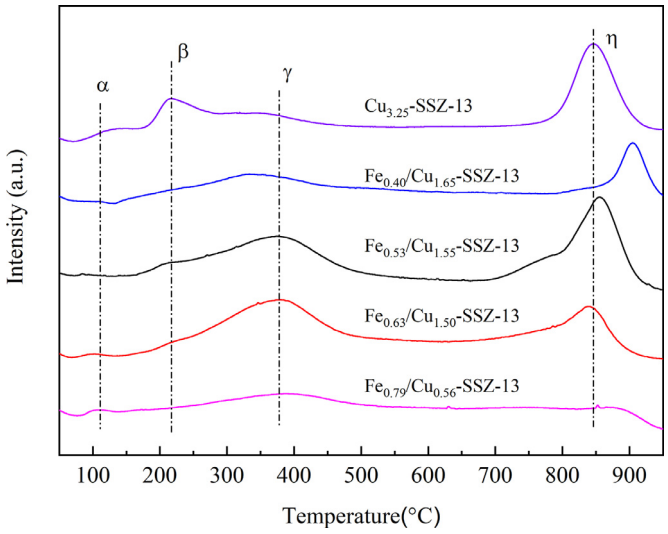

Fig. 2 – H_2 temperature-programmed reductions (H_2-TPR) profiles of the obtained Fe/Cu-SSZ-13 catalysts.

Cu^{2+} (Cu^{2+}-IV) near octatomic ring window (site IV); peak β (249°C) represents the reduction of isolated Cu^{2+} (Cu^{2+}-I) in the super-cage deviating from the double hexatomic ring (site I); peak γ (366°C) represents the reduction of isolated Cu^{2+} (Cu^{2+}-III) centered in the hexagonal prism (sites III); While peak η (>700°C) reflects the reduction of ionic Cu^{+} to metallic Cu^{0} (Gualtieri et al., 2006; Kwak et al., 2012; Chen et al., 2018). It worth mention that Borfecchia reported Cu^{2+} species would undergo "self-reduction" (Borfecchia et al., 2015) to Cu^{+} in inert atmosphere, thus the H_2 consumption in H_2-TPR profiles at low temperatures may not contain all the copper species due to N_2 pretreatment before H_2-TPR tests. But considering the distinctively different reduction temperatures (above 700°C for Cu^{+} vs below 400°C for Cu^{2+}), it is reasonable to say the H_2-TPR profiles could still provide support for identifying Cu^{2+} and Cu^{+} species. For Fe-Cu-SSZ-13 catalysts, as Fe content increases, both peak α and β diminish gradually while peak γ is broadened with higher intensity. Since Cu^{2+}-site III species centered in the hexagonal prism possesses the highest stability due to their large steric hindrances, the peak diminishing suggests the disappearance of more active Cu^{2+}-I and Cu^{2+}-IV species due to either lower Cu content or site occupation by introduced Fe species. On the other hand, the reduction temperature of isolated Fe^{3+} species is generally around 350–400°C (Bernard et al., 2000; Kang, 2000), therefore the peak γ broadening can be related to peak overlap due to close reduction temperature between isolated Fe^{3+} species and Cu^{2+}-III species.

2.3. *Surface chemistry by XPS analyses*

Surface element distribution and corresponding chemical states have been investigated by XPS analyses. The obtained XPS spectra along with the peak fitting results are presented in Fig. 3. As can been seen from Fig. 3**a**, all the catalysts exhibit Cu $2p_{3/2}$ (binding energy around 933.0 eV) and Cu $2p_{1/2}$ (binding energy around 952.5.0 eV, not shown in Fig. 3**a**) peaks. The Cu $2p_{3/2}$ transition around 933.0 eV was differentiated into two peaks at 933.2 and 935.4 eV. According to previous reports, the 933.2 eV peak was related to isolated surface Cu^{+} species, while the 935.4 eV peak can be assigned to isolated Cu^{2+} species coordinated with oxygen atoms in the SSZ-13 framework (Liu and Emiel, 2013; Han et al., 2017; Zhang and Yang, 2018). Fig. 3**b** shows the XPS spectra of Fe 2p, as two characteristic peaks of Fe $2p_{3/2}$ and Fe $2p_{1/2}$ located around 710.0 and 723 eV can be observed. The Fe $2p_{3/2}$ peak was differentiated into two main peaks (710.0 and 713.4 eV), which are very closed to the Fe $2p_{3/2}$ binding energies in FeO and Fe_2O_3, suggesting that the Fe ions exist in forms of Fe^{2+} and Fe^{3+} respectively (Stanislaw et al., 2007; Brandenberger et al., 2010). It's worth noticing that for $Fe_{0.79}/Cu_{0.56}$-SSZ-13, the binding energy of Fe^{3+} shows a clear shift to lower positions at 711.7 eV, which can be related to the formation of partially agglomerated Fe_2O_3 (Brandenberger et al., 2010; Zhang and Yang, 2018). A very rough semi-quantification of Cu^{2+} content was also calculated based on the XPS results by comparing the corresponding peak areas It can be seen in Table 1 that with increased Fe loading, the total amount of Cu species on the catalysts surfaces gradually decreases. Besides, the Cu^{2+} content is obviously lower the Cu+ content, suggesting the Cu^{2+} species are mostly coordinated in different sites insides the zeolites CHA structure, which is in consist with H_2-TPR analyses. The $Cu^{2+}/(Cu^{2+}+Cu^{+})$ ratio also decreases with increased Fe loading, suggesting these coordinating sites could be occupied upon Fe doping.

Table 1 – Surface element distributions in the Fe/Cu-SSZ-13 catalysts.

Sample	Cu (at.%)	Fe (at.%)	$Cu^{2+}/(Cu^{2+}+Cu^{+})$ (%)
$Cu_{2.25}$-SSZ-13	0.79	–	12.7%
$Fe_{0.40}/Cu_{1.65}$-SSZ-13	0.68	0.15	10.3%
$Fe_{0.53}/Cu_{1.55}$-SSZ-13	0.61	0.18	9.8%
$Fe_{0.63}/Cu_{1.50}$-SSZ-13	0.58	0.22	8.6%
$Fe_{0.79}/Cu_{0.56}$-SSZ-13	0.51	0.10	3.9%

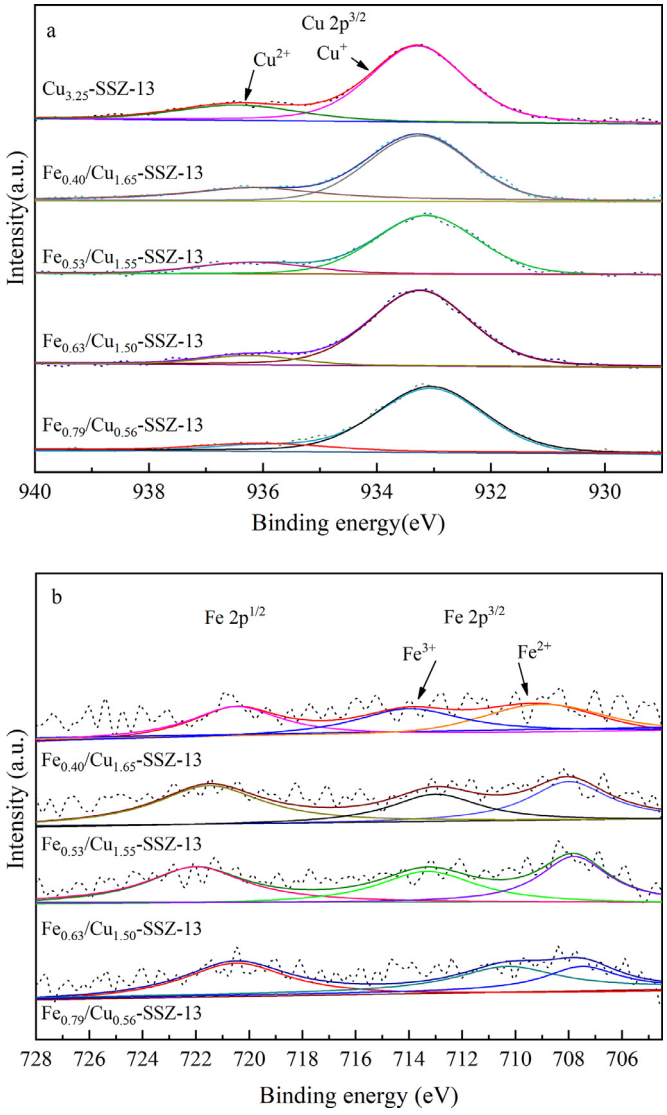

Fig. 3 – (a) Cu 2p and (b) Fe 2p X-ray photoelectron spectra (XPS) of the obtained Fe/Cu-SSZ-13 catalysts with different Fe content.

2.4. *Identification of Fe species by UV–Vis analyses*

UV–Vis analyses were conducted to gain further insights on the chemical states and elemental distribution of Fe species in the Fe/Cu-SSZ-13 catalysts. The obtained spectra (Fig. 4a) with the deconvolution results (Fig. 4b) are presented below. For all the Fe/Cu-SSZ-13 catalysts, three types of iron species can be generally recognized. Two bands at 220–225 and 270–277 nm can be both assigned to the isolated Fe^{3+} species, as the former can be attributed to the tetrahedral Fe^{3+}-I occupying the ion-exchanging positions, while the latter can be attributed to the octahedral Fe^{3+}-II coordinated into the zeolite framework. The bands at 345 nm are related to oligomeric Fe_xO_y species while the bands above 400 nm are related to agglomerated Fe_2O_3 large particles outside the SSZ-13 surface (Lu et al., 2005; Brandenberger et al., 2009, 2010). With increasing Fe content, these two bands at 345 and 410 nm become more prominent. The relative proportion of different Fe species is quantitatively calculated based the deconvoluted spectra (Table 2). It clearly demonstrates that the nature and distribution of the iron species change with increasing Fe loading content. At lower Fe loading content (0.40 wt.%), the monomeric Fe^{3+} species prove to be predominant; while at higher Fe content, the content of monomeric Fe^{3+} species gradually decreases and formation of larger iron species such as oligomeric Fe_xO_y and agglomerated Fe_2O_3 occurs. Such iron species evolution can be explained as follows: at low Fe content, most of the introduced Fe tends to occupy either charge-compensation position of proton H^+ sites or the Al^{3+} sites in the zeolite framework; with increasing Fe loading, these H^+ and Al^{3+} sites gradually become saturated and more difficult to occupy, thus Fe tends to form different surface aggregated species and the relative proportion of monomeric Fe^{3+} species gradually drops.

The above results have demonstrated the successful one-pot synthesis of Fe/Cu-SSZ-13 catalysts. By adjusting Fe loading content properly, the synthesized Fe/Cu-SSZ-13 catalysts

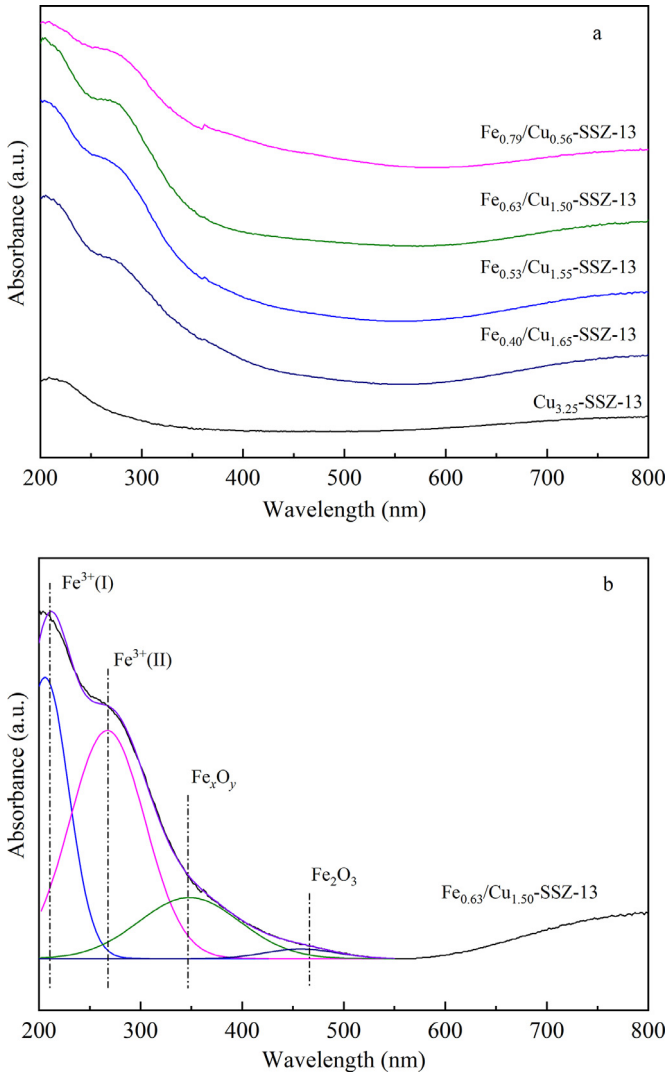

Fig. 4 – (a) Ultraviolet visible spectra (UV–Vis) of Fe/Cu-SSZ-13 catalysts and (b) deconvoluted spectra of the $Fe_{0.63}/Cu_{1.50}$-SSZ-13 catalyst.

Table 2 – Relative proportion of different Fe species in the Fe/Cu-SSZ-13 catalysts.

Sample	Monomeric Fe^{3+}-I (at.%)	Monomeric Fe^{3+}-II (at.%)	Oligomeric Fe_xO_y (at.%)	Fe_2O_3 (at.%)
$Fe_{0.40}/Cu_{1.65}$-SSZ-13	28.85	44.63	22.53	3.990
$Fe_{0.53}/Cu_{1.55}$-SSZ-13	24.32	43.09	28.13	4.460
$Fe_{0.63}/Cu_{1.50}$-SSZ-13	22.26	41.89	33.01	2.840
$Fe_{0.79}/Cu_{0.56}$-SSZ-13	12.89	29.92	35.17	22.52

Fe^{3+}-I: tetrahedral Fe^{3+} occupying the ion-exchanging positions; Fe^{3+}-II: octahedral Fe^{3+} coordinated into the zeolite framework.

present typical CHA structure with good crystallinity similar to the Cu-SSZ-13 catalysts, but Fe over-doping would lead to severe damage of the zeolite structure. Further characterizations revealed that isolated Cu^{2+} and monomeric Fe^{3+} are revealed to be the predominant Fe and Cu species in the Fe/Cu-SSZ-13 catalysts, whereas isolated Cu^{2+} locates at three different sites (Cu^{2+}-IV, Cu^{2+}-I and Cu^{2+}-III) in the CHA structure, and monomeric Fe^{3+} locates at two different sites (Fe^{3+}-I and Fe^{3+}-II) in the CHA structure. With increasing Fe content, more active Cu^{2+}-I and Cu^{2+}-IV gradually disappear, along with the formation of oligomeric Fe_xO_y and agglomerated Fe_2O_3.

2.5. *Catalytic performance of catalysts*

2.5.1. *NH_3-SCR activity*

Fig. 5 shows the NO_x conversions over Fe/Cu-SSZ-13 catalysts during NH_3-SCR tests. As can be seen, the operation temperature window width (the corresponding temperature ranges while the conversion of NO_x is above 90%) follows the or-

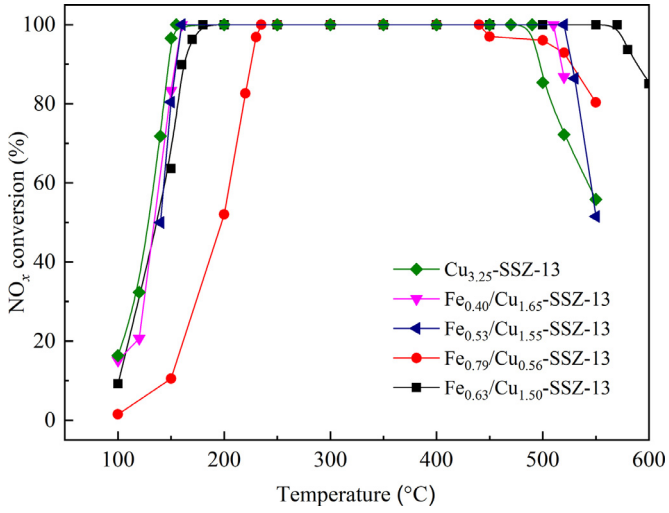

Fig. 5 – NO_x conversion over the obtained Fe/Cu-SSZ-13 catalysts.

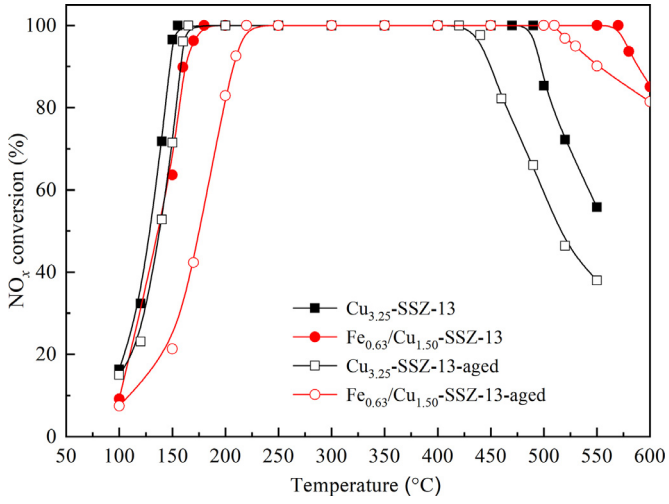

Fig. 6 – NO_x conversion over $Cu_{3.25}$-SSZ-13 and $Fe_{0.63}/Cu_{1.50}$-SSZ-13 catalysts before/after hydro-thermal aging.

der as: $Fe_{0.63}/Cu_{1.50}$-SSZ-13 (160–580°C) > $Fe_{0.53}/Cu_{1.55}$-SSZ-13 (155–530°C) > $Fe_{0.40}/Cu_{1.65}$-SSZ-13 (160–520°C) > $Cu_{3.25}$-SSZ-13 (145–490°C) > $Fe_{0.79}/Cu_{0.56}$-SSZ-13 (220–500°C). Comparing with single $Cu_{3.25}$-SSZ-13, although the temperature value of 90% NO_x conversion (T_{90}) has no obvious change at lower temperatures, the high temperature activity of Fe/Cu-SSZ-13 (with about 1.55 wt.% Cu) is significantly improved with increasing Fe content. It is worth noticing that the $Fe_{0.63}/Cu_{1.50}$-SSZ-13 catalyst with 0.63 wt.% Fe content presents the widest operation temperature window from 160 to 580°C, as the NO_x conversion can be maintained above 90% even at 580°C, which suggests its clear advantages in actual applications. However, upon further increasing the Fe content, both high temperature and low temperature activity decreases significantly for the $Fe_{0.79}/Cu_{0.56}$-SSZ-13 catalysts with 0.79 wt.% Fe, resulting in the narrowest operation temperature window. Such deteriorating result can be caused by either the decrease of Cu content owing to sites occupation by Fe^{2+}, or the damage of the zeolite structure due to substitution of Al^{3+} in the tetrahedral coordination structure by Fe^{3+} ions. Besides, the NH_3-SCR performances of Fe/Cu-SSZ-13 and Cu-SSZ-13 with similar Cu loadings were also evaluated by subjecting $Fe_{0.63}/Cu_{1.50}$-SSZ-13, $Cu_{3.25}$-SSZ-13 and $Cu_{1.79}$-SSZ-13 to same NH_3-SCR test protocols, and the results (Appendix A **Fig. S2**) further demonstrated the superiority of Fe/Cu-SSZ-13 catalyst. Moreover, regarding the affection of different space velocity, our previous studies (Chen et al., 2018) on Cu-SSZ-13 catalyst (Appendix A **Fig. S3**) as well as various reports (Zhang et al., 2015) have all demonstrated the excellent adaptability to high GHSV of Cu-SSZ-13 and FeCu-SSZ-13 based catalysts, suggesting its promising application in diesel-engines exhaust purification.

2.5.2. *Hydro-thermal stability*

Fig. 6 shows the NO_x conversions over $Fe_{0.63}/Cu_{1.50}$-SSZ-13 and $Cu_{3.25}$-SSZ-13 catalysts upon hydro-thermal aging treatment. For the single $Cu_{3.25}$-SSZ-13 sample, the operation temperature window is significantly narrowed upon hydro-thermal aging (145–490°C before aging and 160–450°C after aging). For $Fe_{0.63}/Cu_{1.50}$-SSZ-13 catalysts, the operation temperature window can be retained from 205 to 550°C. Although the low

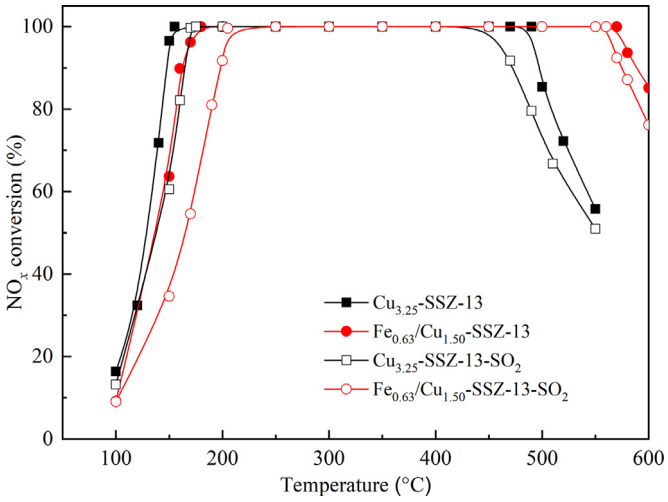

Fig. 7 – NO_x conversion over $Fe_{0.63}/Cu_{1.50}$-SSZ-13 and $Cu_{3.25}$-SSZ-13 catalysts before/after SO_2 pretreatment.

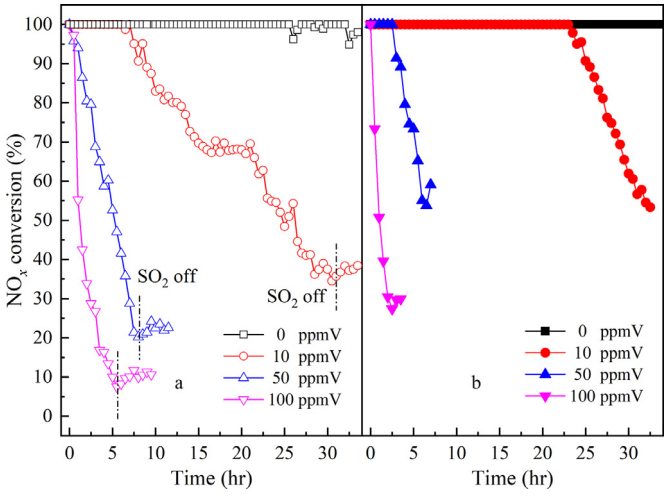

Fig. 8 – Effect of different SO_2 concentration in the reaction feed gas on denitrification performance of (a) $Cu_{3.25}$-SSZ-13 and (b) $Fe_{0.63}/Cu_{1.50}$-SSZ-13 catalysts.

temperature activity was deteriorated to a certain degree, $Fe_{0.63}/Cu_{1.50}$-SSZ-13 still presents excellent high temperature activity with wider operation temperature window upon hydrothermal aging.

2.5.3. *Anti-sulfur performance*

Sulfur poisoning has long been a critical challenge that demands consideration during the practical application of the SCR catalysts. Therefore, the affection of sulfur-poisoning on the de NO_x performance of $Cu_{3.25}$-SSZ-13 and $Fe_{0.63}/Cu_{1.50}$-SSZ-13 catalysts were also evaluated. As shown in Fig. 7, after 16 hr treating in SO_2 at 350°C, the operation temperature window of $Cu_{3.25}$-SSZ-13 occurs from 165 to 470°C, while the temperature window of $Fe_{0.63}/Cu_{1.50}$-SSZ-13 occurs from 200 to 570°C. Similar to the effect of hydrothermal aging, although the low temperature activity was also deteriorated, $Fe_{0.63}/Cu_{1.50}$-SSZ-13 still presents excellent high temperature activity with wider operation temperature window, especially its T_{90} value at high temperature was only decreased by 10°C. Such results indicate that $Fe_{0.63}/Cu_{1.50}$-SSZ-13 shows an outstanding sulfur resistance and was potentially preferable for practical application.

Additionally, to better simulate real working condition of diesel engine vehicles, the tolerability of $Cu_{3.25}$-SSZ-13 (Fig. 8a) and $Fe_{0.63}/Cu_{1.50}$-SSZ-13 (Fig. 8b) catalysts exposed to NO_x-NH_3-O_2 feed gas with different SO_2 concentrations was also evaluated. As can be seen, NH_3-SCR activity of both samples can be quite stable and NO_x conversion remains at around 100% as in the NO_x-NH_3-O_2 reaction feed gas. Once SO_2 is introduced, NO_x conversion over both catalysts drops immediately and sharply. Higher concentration of SO_2 in the reaction feed gas lead to more severe NH_3-SCR activity deterioration. For $Cu_{3.25}$-SSZ-13 catalyst, NO_x conversion can be maintained at 100% for about 6 hr with 10 ppmV SO_2 and after 30 hr reaction only 35% NO_x conversion can be retained; when SO_2 concentration increases above 50 ppmV, NO_x conversion drops below 50% in less than 5 hr, indicating its poor tolerability against sulfur poisoning. For $Fe_{0.63}/Cu_{1.50}$-SSZ-13 cat-

alyst, NO_x conversion can be maintained at 100% for about 22 hr with 10 ppmV SO_2 and over 50% NO_x conversion can be retained after 30 hr reaction; when SO_2 concentration increases to 50 ppmV, NO_x conversion can remain at 100% for the first 5 hr. These results show that the anti-sulfur performance of $Fe_{0.63}/Cu_{1.50}$-SSZ-13 catalyst is significantly improved by proper Fe doping. Moreover, when SO_2 is switched off in the feed gas, NO_x conversion over both catalysts was not able to recover to the initial level. This suggests that the sulfur poisoning phenomenon does not originate from the competitive adsorption between SO_2 and reaction gas, instead it is more likely related to the permanent block of surface active sites by $(NH_4)_2SO_4$ and NH_4HSO_4 species formed on the catalyst surface (Pieterse et al., 2006; Jin et al., 2014). Our previous study on Cu-SSZ-13 series (Chen et al., 2018) have also deomonstrated the existence of $(NH_4)_2SO_4$ and NH_4HSO_4 on the catalyst surface after SO_2 resistance test at 155°C for 30 hr via thermogravimetry-differential scanning calorimetry (TG-DSC) analyses (Appendix A **Fig. S4**). The affection of sulfur poisoning on active species such as isolated Cu^{2+} and monomeric Fe^{3+} required further in-depth studies and was not discussed in this work. In our previous study on Cu-SSZ-13 series (Chen et al., 2018), electron paramagnetic resonance (EPR) profiles of SO_2 pretreated Cu-SSZ-13 samples shows that the coordination environment of Cu^{2+} species wasn't changed a lot and major content of isolated Cu^{2+} can be retained after SO_2 pretreatment. Therefore, we can generally assume that SO_2 pretreatments does not show significant impact on active species.

Combining the catalytic performance results above, it is well demonstrated that appropriate amount of Fe doping of Fe/Cu-SSZ-13 catalysts can improve NH_3-SCR activity at expanded operation temperature window as well as enhance it tolerability against hydrothermal aging and SO_2 poisoning, making the optimized Fe/Cu-SSZ-13 catalyst system promising for potential industrial applications. The results of systematic characterizations also suggest that the catalytic behaviors of Fe-Cu-SSZ-13 catalysts should be related to the nature of Cu and Fe species, therefore, comparison and correlations between active Cu/Fe species and catalytic activities are discussed in the following discussion in order to acquire deeper insights regarding the structure-activity relationship of Fe/Cu-SSZ-13 catalysts for NH_3-SCR reaction.

2.6. *Correlations between active species and catalytic activities*

Extensive studies have been previously reported on Cu-zeolites catalysts for NH_3-SCR reactions. A series of stable Cu species have been reported to be active sites including isolated Cu ions, dimeric Cu species and even agglomerated CuO_x clusters. Wang proposed isolated Cu ions coordinated at ion-exchange sites are more likely to be the active sites rather than CuO, as CuO not only shows weak interaction with acid sites in the zeolites structure but also accelerates the NH_3 oxidation at high temperatures, leading to lower NH_3-SCR reaction activity (Wang et al., 2012, 2013). Giordanino et al. (2013) revealed that dimeric Cu species scarcely exist in Cu-SSZ-13 framework and are very unlikely to be active species. Our previous research on Cu-SSZ-13 catalysts revealed three different forms of isolated Cu^{2+} species in the CHA structure, and these isolated Cu^{2+} species are beneficial for improving low-temperature NH_3-SCR activity (Chen et al., 2018). In the present work, isolated Cu^{2+} species and Cu^+ are validated as the predominant copper species, while dimeric Cu species and CuO_x clusters are not observed. Cu^+ presents high reduction temperature above 700°C, thus can also be ruled out as active sites. Therefore, it is reasonable to say that higher catalytic reactivity (especially at low temperatures) of Cu-SSZ-13 catalyst can be attributed to the isolated Cu^{2+} species. With increasing Fe content in Fe/Cu-SSZ-13 catalysts, part of the isolated Cu^{2+} disappeared due to low Cu content or site occupation by introduced Fe. Therefore, the low temperature NH_3-SCR activities are slightly hindered in Fe/Cu-SSZ-13, as demonstrated in activity tests.

For Fe species, various types of iron species have also been proposed to be active sites in previous studies, such as monomeric iron ions, oligomeric Fe_xO_y and even large Fe_2O_3 particles. Høj et al. (2009) proposed that monomeric iron ions should be the predominant iron species under low (<1.2 wt.%) iron loading conditions. Devadas et al. (2007) suggested that the rate-determining step is NO oxidation and Fe_2O_3 particles with high oxidizing ability should be critical active sites. However, Shwan et al. (2012) demonstrated that the increased ability of NO oxidation does not necessarily result in increased NH_3-SCR activity, on the contrary it would cause undesired ammonia oxidation hindering SCR reaction. Further studies by Yin et al. (2016) and Liu et al. (2015) all proposed that the monomeric iron ions are major contributor to the high temperature SCR activity of Fe-Cu-SSZ-13 catalysts. Zhang et al. (2015) suggested it is possible to control the temperature window range for NO conversion by controlling the content of Cu and Fe species, as the presence of more copper species seems to be helpful whereas at high temperatures the presence of more iron species is desired. In the present work, monomeric Fe^{3+} located at two different sites (Fe^{3+}-I and Fe^{3+}-II) in the CHA structure are validated as the predominant iron species. Based on the above literatures and results, we may conclude that for Fe-Cu-SSZ-13 catalysts, isolated Cu^{2+} species act as primary active sites for low temperature SCR reaction, while monomeric Fe^{3+} species provide sufficient active sites for sustain the SCR activity at high temperature. Therefore, the operation temperature window of Fe-Cu-SSZ-13 is significantly expanded comparing to Cu-SSZ-13. Moreover, for $Fe_{0.79}/Cu_{0.56}$-SSZ-13, Fe over doping leads to the damage of zeolite structure, destruction of isolated Cu^{2+} site, as well as the formation of highly oxidizing Fe_2O_3, thus it presents worst catalytic performances.

3. Conclusions

Fe/Cu-SSZ-13 zeolites with different Fe loading content were successfully synthesized with one-pot strategy and evaluated for NH_3-SCR reactivity. Textural analysis of the catalysts reveals that the synthesized Fe/Cu-SSZ-13 catalysts present typical CHA structure with good crystallinity. Isolated Cu^{2+} and monomeric Fe^{3+} are identified as the predominant copper and iron species. The activity evaluation results show that $Fe_{0.63}/Cu_{1.50}$-SSZ-13 catalyst with proper Fe content shows outstanding SCR activity over wide temperature range from

160 to 580°C, along with high hydrothermal stability as well as good SO_2 resistance. The improvement of catalytic behaviors of Fe/Cu-SSZ-13 can be correlated to the nature of active species iron and copper species, as isolated Cu^{2+} species act as primary active sites for low temperature SCR reaction, while monomeric Fe^{3+} species provide sufficient active sites for sustain the SCR activity at high temperature. Moreover, Fe over doping can result in deteriorated catalytic performances, due to the damage of zeolite structure, destruction of isolated Cu^{2+} site, as well as the formation of highly oxidizing Fe_2O_3.

Acknowledgments

This work was supported by the Key Program of Science Technology Department of Zhejiang Province (No. 2018C03037) and the Scientific Research Fund of Nanjing Institute of Technology (No. YKJ2019111).

Appendix A. Supplementary data

Supplementary material associated with this article can be found in the online version at doi:10.1016/j.jes.2020.08.003.

REFERENCES

Bernard, C., Mathias, M., Gérard, D., 2000. Kinetics and mechanism of the N_2O reduction by NH_3 on a Fe-zeolite-beta catalyst. J. Catal. 195 (2), 298–303.

Borfecchia, E., Lomachenko, K.A., Giordanino, F., Falsig, H., Beato, P., Soldatov, A.V., et al., 2015. Revisiting the nature of Cu sites in the activated Cu-SSZ-13 catalyst for SCR reaction. Chem. Sci. 6 (1), 548–563.

Brandenberger, S., Kröcher, O., Wokaun, A., Tissler, A., Althoff, R., 2009. The role of Bronsted acidity in the selective catalytic reduction of NO with ammonia over Fe-ZSM-5. J. Catal. 268 (2), 297–306.

Brandenberger, S., Kröcher, O., Tissler, A., Althoff, R., 2010. The determination of the activities of different iron species in Fe-ZSM-5 for SCR of NO by NH_3. Appl. Catal. B 95 (3–4), 348–357.

Busca, G., Lietti, L., Ramis, G., Berti, F., 1998. Chemical and mechanistic aspects of the selective catalytic reduction of NO_x by ammonia over oxide catalysts: a review. Appl. Catal. B 18 (1–2), 1–36.

Chen, J.W., Zhao, R., Zhou, R.X., 2018. A new insight into active Cu^{2+} species properties in one-pot synthesized Cu-SSZ-13 catalysts for NO_x reduction by NH_3. ChemCatChem 10 (22), 5182–5189.

Deka, U., Juhin, A., Eilertsen, E.A., 2012. Confirmation of isolated Cu^{2+} ions in SSZ-13 zeolite as active sites in NH_3-selective catalytic reduction. J. Phys. Chem. C 116 (7), 4809–4818.

Devadas, M., Kröcher, O., Elsener, M., Wokaun, A., Mitrikas, G., Söger, N., et al., 2007. Characterization and catalytic investigation of Fe-ZSM5 for urea-SCR. Catal. Today 119 (1–4), 137–144.

Epling, W.S., Campbell, L.E., Yezerets, A., Currier, N.W., Parks, J.E., 2004. Overview of the fundamental reactions and degradation mechanisms of NO_x storage/reduction catalysts. Catal. Rev. 46 (2), 163–245.

Gao, F., Wang, Y., Kollár, M., Washton, N.M., Szanyi, J., Peden, C.H.F., 2015a. A comparative kinetics study between Cu/SSZ-13 and Fe/SSZ-13 SCR catalysts. Catal. Today 258, 347–358.

Gao, F., Kollár, M., Kukkadapu, R.K., Washton, N.M., Wang, Y., Szanyi, J., et al., 2015b. Fe/SSZ-13 as an NH_3-SCR catalyst: a reaction kinetics and FTIR/Mössbauer spectroscopic study. Appl. Catal. B 164, 407–419.

Gao, F., Mei, D., Wang, Y., Szanyi, J., Peden, C.H.F., 2017. Selective catalytic reduction over Cu/SSZ-13: linking homo- and heterogeneous catalysis. J. Am. Chem. Soc. 139 (13), 4935–4942.

Garcıá-Cortés, J.M., Pérez-Ramırez, J., Illán-Gómez, M.J., Kapteijn, F., Moulijn, J.A., 2001. Comparative study of Pt-based catalysts on different supports in the low-temperature de-NO_x-SCR with propene. Appl. Catal. B 30 (3–4), 399–408.

Giordanino, F., Vennestrøm, P.N.R., Lundegaard, L.F., Stappen, F.N., Mossin, S., Beato, P., et al., 2013. Characterization of Cu-exchanged SSZ-13: a comparative FT-IR, UV-Vis, and EPR study with Cu-ZSM-5 and Cu-β with similar Si/Al and Cu/Al ratios. Dalton Trans. 42 (35), 12741–12761.

Gualtieri, A.F., Passaglia, E., 2006. Rietveld structure refinement of NH_4-exchanged natural chabazite. Eur. J. Mineral. 18 (3), 351–359.

Han, S., Cheng, J., Zheng, C., Ye, Q., Cheng, S., Kang, T., et al., 2017. Effect of Si/Al ratio on catalytic performance of hydrothermally aged Cu-SSZ-13 for the NH_3-SCR of NO in simulated diesel exhaust. Appl. Surf. Sci. 419, 382–392.

Høj, M., Beier, M.J., Grunwaldt, J.D., Dahl, S., 2009. The role of monomeric iron during the selective catalytic reduction of NO_x by NH_3 over Fe-BEA zeolite catalysts. Appl. Catal. B 93 (1–2), 166–176.

Jin, R., Liu, Y., Wang, Y., Chen, W., Wu, Z., Wang, H., et al., 2014. The role of cerium in the improved SO_2 tolerance for NO reduction with NH_3 over Mn-Ce/TiO_2 catalyst at low temperature. Appl. Catal. B 148-149, 582–588.

Kang, M., 2000. Methanol conversion on metal-incorporated SAPO-34 s (MeAPSO-34 s). J. Mol. Catal. A 160 (2), 437–444.

Kwak, J.H., Zhu, H.Y., Lee, J.H., Peden, C.H.F., Szanyi, J., 2012. Two different cationic positions in Cu-SSZ-13. Chem. Commun. 48 (39), 4758–4760.

König, A., Herding, G., Hupfeld, B., Richter, T., Weidmann, K., 2001. Current tasks and challenges for exhaust aftertreatment research. A viewpoint from the automotive industry. Top. Catal. 16-17 (1), 23–31.

Li, J., Chang, H., Ma, L., Hao, J., Yang, R.T., 2011. Low-temperature selective catalytic reduction of NO_x with NH_3 over metal oxide and zeolite catalysts-A review. Catal. Today 175 (1), 147–156.

Liu, P., Emiel, J.M.H., 2013. Highly efficient and robust $Au/MgCuCr_2O_4$ catalyst for gas-phase oxidation of ethanol to acetaldehyde. J. Am. Chem. Soc. 135 (38), 14032–14035.

Liu, X.J., Li, Y.H., Zhang, R.R., 2015. Ammonia selective catalytic reduction of NO over Ce-Fe/Cu-SSZ-13 catalysts. RSC Adv. 5 (104), 85453–85459.

Liu, J.X., Yu, F.H., Liu, J., Cui, L.F., Zhao, Z., Wei, Y.C., et al., 2016. Synthesis and kinetics investigation of meso-microporous Cu-SAPO-34 catalysts for the selective catalytic reduction of NO with ammonia. J. Environ. Sci. 48, 45–58.

Lu, L., Li, L., Wang, X., Li, G., 2005. Understanding of the finite size effects on lattice vibrations and electronic transitions of nano α-Fe_2O_3. J. Phys. Chem. B 109 (36), 17151–17156.

Nares, R., RamÍrez, J., Gutiérrez-Alejandre, A., Louis, C., Klimova, T., 2002. Ni/Hβ-zeolite catalysts prepared by deposition-precipitation. J. Phys. Chem. B 106 (51), 13287–13293.

Pieterse, J., Top, H., Vollink, F., Hoving, K., Vanderbrink, R., 2006. Selective catalytic reduction of NO_x in real exhaust gas of gas engines using unburned gas: catalyst deactivation and advances toward long-term stability. Chem. Eng. J. 120 (1–2), 17–23.

Qi, G.S., Wang, Y.H., Yang, R.T., 2008. Selective catalytic reduction of nitric oxide with ammonia over ZSM-5 based catalysts for diesel engine applications. Catal. Lett. 121 (1–2), 111–117.

Ren, L.M., Zhu, L.F., Yang, C.G., Chen, Y.M., Sun, Q., Zhang, H.Y., et al., 2011. Designed copper-amine complex as an efficient template for one-pot synthesis of Cu-SSZ-13 zeolite with excellent activity for selective catalytic reduction of NO_x by NH_3. Chem. Commun. 47, 9789–9791.

Shishkin, A., Kannisto, H., Carlsson, P.A., Härelind, H., Skoglundh, M., 2014. Synthesis and functionalization of SSZ-13 as an NH_3-SCR catalyst. Catal. Sci. Technol. 4 (11), 3917–3926.

Shwan, S., Nedyalkova, R., Jansson, J., Korsgren, J., Olsson, L., Skoglundh, M., 2012. Hydrothermal stability of Fe-BEA as an NH_3-SCR catalyst. Ind. Eng. Chem. Res. 51 (51), 12762.

Si, Z.C., Weng, D., Wu, X.D., Li, J., Li, G., 2010. Structure, acidity and activity of CuO_x/WO_x-ZrO_2 catalyst for selective catalytic reduction of NO by NH_3. J. Catal. 271 (1), 43–51.

Stanislaw, D., Lorenzo, S., Friedrich, E., 2007. Effect of preparation and metal content on the introduction of Fe in BEA zeolite, studied by DR UV-vis, EPR and Mössbauer spectroscopy. J. Phys. Chem. Solids 68 (10), 1885–1891.

Wang, L., Li, W., Qi, G.S., Weng, D., 2012. Location and nature of Cu species in Cu/SAPO-34 for selective catalytic reduction of NO with NH_3. J. Catal. 289, 21–29.

Wang, L., Gaudet, J.R., Li, W., Weng, D., 2013. Migration of Cu species in Cu/SAPO-34 during hydrothermal aging. J. Catal. 306 (1–2), 68–77.

Wang, J.C., Peng, Z.L., Chen, Y., 2015. In-situ hydrothermal synthesis of Cu-SSZ-13/cordierite for the catalytic removal of NO_x from diesel vehicles by NH_3. Chem. Eng. J. 263, 9–19.

Wang, Y.J., Xie, L.J., Liu, F.D., Ruan, W.Q., 2019. Effect of preparation methods on the performance of CuFe-SSZ-13 catalysts for selective catalytic reduction of NO_x with NH_3. J. Environ. Sci. 81, 195–204.

Wen, C., Geng, L., Han, L., Wang, J., Chang, L., Feng, G., et al., 2015. A comparative first principles study on trivalent ion incorporated SSZ-13 zeolites. Phys. Chem. Chem. Phys. 17 (44), 29586–29596.

Yin, C.Y., Cheng, P.F., Li, X., Yang, R.T., 2016. Selective catalytic reduction of nitric oxide with ammonia over high-activity Fe/SSZ-13 and Fe/one-pot-synthesized Cu-SSZ-13. Catal. Sci. Technol. 6 (20), 7561–7568.

Zhang, T., Li, J., Liu, J., Wang, D., Zhao, Z., Cheng, K., et al., 2015. High activity and wide temperature window of Fe-Cu-SSZ-13 in the selective catalytic reduction of NO with ammonia. AIChE J. 61 (11), 3825–3837.

Zhang, D., Yang, R.T., 2018. N_2O formation pathways over zeolite-supported Cu and Fe catalysts in NH_3-SCR. Energ. Fuel 32 (2), 2170–2182.

Zhang, D.J., Ma, Z.R., Wang, B.D., Zhu, T., Weng, D., Wu, X.D., et al., 2019. $V_xMn_{(4-x)}Mo_3Ce_3$/Ti catalysts for selective catalytic reduction of NO by NH_3. J. Environ. Sci. 88, 145–154.

Zones, S.I., Vannordstrand, R.A., 1988. Novel zeolite transformations: the template mediated conversion of cubic-P zeolite to SSZ-13. Zeolites 8, 166–174.